A&A 374, 1056–1070 (2001)
DOI: 10.1051/0004-6361:20010794

Astronomy & Astrophysics

V 1162 Ori: A multiperiodic δ Scuti star with variable period and amplitude⋆,⋆⋆

T. Arentoft[1], C. Sterken[1,⋆⋆⋆], G. Handler[2], L. M. Freyhammer[1,3], A. Bruch[4], P. Niarchos[5], K. Gazeas[5], V. Manimanis[5], P. Van Cauteren[6], E. Poretti[7], D. W. Dawson[8,9], Z. L. Liu[10], A. Y. Zhou[10], B. T. Du[10], R. R. Shobbrook[11], R. Garrido[12], R. Fried[13], M .C. Akan[14], C. Ibanoglu[14], S. Evren[14], G. Tas[14], D. Johnson[8], C. Blake[15], and D .W. Kurtz[16,17,18]

[1] University of Brussels (VUB), Pleinlaan 2, 1050 Brussels, Belgium
[2] South African Astronomical Observatory, PO Box 9, Observatory 7935, South Africa
[3] Royal Observatory of Belgium, Ringlaan 3, 1180 Brussels, Belgium
[4] Laboratório Nacional de Astrofísica, CP 21, 37500-000 Itajubá – MG, Brazil
[5] Department of Astrophysics, Astronomy and Mechanics, University of Athens, 157 84 Zografos, Athens, Greece
[6] Beersel Hills Observatory, Belgium
[7] Osservatorio Astronomico di Brera, Via E. Bianchi 46, 23807 Merate, Italy
[8] Department of Astronomy, San Diego State University, San Diego, California, USA
[9] Department of Physics and Astronomy, Western Connecticut State University, Danbury, Connecticut 06810, USA
[10] Beijing Astronomical Observatory, Chinese Academy of Sciences, Beijing 100012, PR China
[11] Research School of Astronomy and Astrophysics, Australian National University, Weston Creek PO, ACT 2611, Australia
[12] Instituto de Astrofisica de Andalucia, CSIC, Apdo. 3004, 18080 Granada, Spain
[13] Braeside Observatory, Flagstaff, Arizona, USA
[14] Ege University Observatory, Bornova 35100, Izmir, Turkey
[15] Astrophysical Sciences Department, Princeton University, Princeton, New Jersey 08544, USA
[16] Centre for Astrophysics, University of Central Lancashire, Preston PR1 2HE, UK
[17] Department of Astronomy, University of Cape Town, Rondebosch 7701, South Africa
[18] Laboratoire d'Astrophysique, Observatoire Midi-Pyrénées, 31400 Toulouse, France

Received 26 April 2001 / Accepted 31 May 2001

Send offprint requests to: T. Arentoft,
e-mail: tarentof@vub.ac.be

⋆ Based on observations obtained at the South African Astronomical Observatory (SAAO), Athens University and Kryonerion Observatories, European Southern Observatories (ESO: applications ESO 62H-0110, 64H-0065 and 64L-0182), Laboratório Nacional de Astrofísica (Brazil), Xinglong, Beersel Hills, Ege University, San Pedro Martir, Merate, Mt. Laguna, Siding Spring, Sierra Nevada, Braeside and Lick Observatories.

⋆⋆ Table 2 is only available in electronic form at the CDS via anonymous ftp to cdsarc.u-strasbg.fr (130.79.128.5) or via
http://cdsweb.u-strasbg.fr/cgi-bin/qcat?J/A+A/374/1056

⋆⋆⋆ Research Director, Belgian Fund for Scientific Research (FWO).

Abstract. We present the results of multisite observations of the δ Scuti star V 1162 Ori. The observations were done in the period October 1999 – May 2000, when 18 telescopes at 15 observatories were used to collect 253 light extrema during a total of 290 hours of time–series observations. The purpose of the observations was to investigate amplitude and period variability previously observed in this star, and to search for low–amplitude frequencies. We detect, apart from the main frequency and its two first harmonics, four additional frequencies in the light curves, all with low amplitudes (1–3 mmag). Combining the present data set with data obtained in 1998–99 at ESO confirms the new frequencies and reveals the probable presence of yet another pulsational frequency. All five low–amplitude frequencies are statistically significant in the data, but at least one of them (f_5) suffers from uncertainty due to aliasing. Using colour photometry we find evidence for a radial main frequency (f_1), while most or all low–amplitude frequencies are likely non–radial. We show that the main frequency of V 1162 Ori has variable amplitude and period/phase, the latter is also displayed in the O–C diagram from light extrema. The amplitude variability in our data is cyclic with a period of 282 d and a range of nearly 20 mmag, but earlier amplitude values quoted in the literature cannot be explained by this cyclic variation. O–C analysis including data from the literature show that the period of V 1162 Ori displays a linear period change as well as sudden or cyclic variations on a time scale similar to that of the amplitude variations.

Key words. stars: variables: δ Scuti – stars: individual: V 1162 Orionis – techniques: photometric – methods: data analysis

1. Introduction

The δ Scuti stars are pulsating A–F stars situated on or just above the main sequence. They display a large range in pulsational amplitude, from the mmag level observed in the low–amplitude, multiperiodic δ Scuti stars up to almost one magnitude found in some of the high–amplitude δ Scuti stars (HADS). The HADS generally have amplitudes exceeding $0\overset{\mathrm{m}}{.}3$ and slow rotational velocities ($v \sin i$ below 30 km s^{-1}). V 1162 Ori is often considered a HADS, although it does not qualify as such due to its full amplitude of only $0\overset{\mathrm{m}}{.}1$–$0\overset{\mathrm{m}}{.}2$ and its high projected rotational velocity ($v \sin i$ of 46 km s^{-1}, Solano & Fernley 1997). It is an intermediate amplitude, up to now monoperiodic Pop I δ Scuti star with a frequency of 12.7082 d^{-1}: Hintz et al. (1998) claimed a secondary frequency near 16.5 d^{-1}, but this was later shown to arise from a variable comparison star (Lampens & Van Cauteren 2000). We will, however, show that V 1162 Ori is not monoperiodic and that it is indeed positioned in the narrow HADS instability strip given by McNamara (2000). V 1162 Ori has in the past shown very large amplitude changes, ranging from half peak–to–peak values of 98 mmag observed by Poretti et al. (1990) to 50 mmag observed by Hintz et al. (1998), who also detected a period break using O–C analysis of times of maximum light. Later changes observed by Arentoft & Sterken (2000, hereinafter Paper I) could be due to period breaks or cyclic period changes, and also these authors detected amplitude variations. As a result it was decided to organise a multisite campaign on V 1162 Ori, spanning a full observing season. The aims were to investigate the time scales of the changes, how or if the amplitude and period/phase variations are related and if possible to gain information on the underlying physical processes causing them. Although amplitude and period variations are common phenomena in δ Scuti stars, the causes are far from understood (see e.g. Breger & Pamyatnykh 1998; Breger 2000a). Even the involved time scales are very different from star to star: 4 CVn, for example, shows amplitude variability on time scales of years (Breger 2000b), whereas XX Pyx displays period and amplitude variability on time scales as short as 20 d (Handler et al. 2000). Breger (2000a) discusses the possibility that amplitude variability can be related to multiperiodicity, as the monoperiodic HADS appear to have more stable amplitudes (e.g. Rodriguez 1999) than the multiperiodic δ Scuti stars of low and possibly also high amplitude.

The philosophy of the present multisite campaign is different from *normal* campaigns on δ Scuti stars: the aim was to collect as many extrema as possible over the observing season (8 months). Thus, the participating teams observed V 1162 Ori whenever they had sufficient time to spare to cover an extremum. These observations, which often covered short light curve sections – sometimes only 20 min – had the purpose of following the evolution of the main pulsational period, and were complemented with dedicated time–series observations from several sites, also distributed over the long time span. The latter allow us to monitor amplitude changes as well as to search for low–amplitude frequencies – however without the usual multisite advantage of suppressed side–lobes in the amplitude spectra.

Finding low–amplitude frequencies is very important for understanding changes in the light curve: low–amplitude frequencies can interfere with the main mode and cause e.g. amplitude variations through beating or give rise to cycle–to–cycle variations. Furthermore, detection of additional pulsation frequencies would yield tighter constraints on stellar models.

2. The data

Data were obtained with 18 different telescopes at 15 sites in 12 countries, utilising both CCDs and PMTs. For the CCD observations, care was taken to avoid having the very bright and close–by star υ Ori on the frames by placing V 1162 Ori near the edge of the field of view. For PMT observations the disturbing effect of a close (10″), $3\overset{\mathrm{m}}{.}1$ fainter neighbouring star on the observational noise was minimised by including the star in the aperture. The observations were, with few exceptions, done through the Johnson V filter. The list of participating observers and

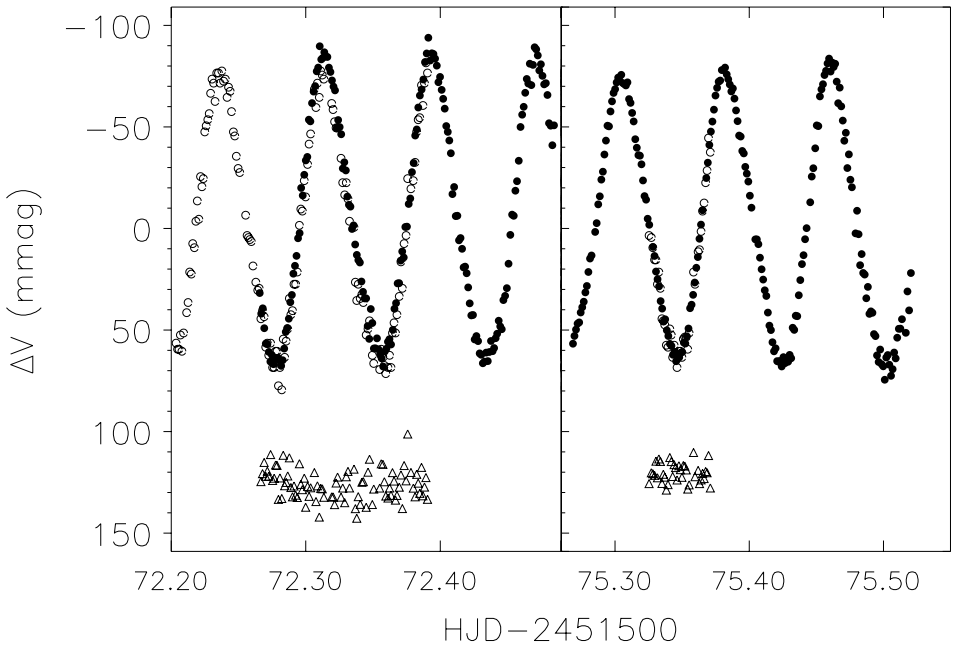

Fig. 1. Examples of light curves obtained in two of the cases of overlapping data. Dots are data from SAAO, open circles data from Athens University Observatory. We also show the difference between the datapoints from Athens and interpolated values of the SAAO datapoints (triangles, shifted by 120 mmag).

sites is given in Table 1, where we also give the number of extrema and hours of data collected with each telescope.

The bulk of the data was reduced by the individual observing teams, and several different reduction procedures were therefore applied. It is beyond the scope of the present paper to describe them all, we will just add that the applied procedures follow general and established methods for reduction of CCD and PMT data. Differential magnitudes were, both for the CCD and PMT data, measured with respect to the star GSC 4478–0019, which is slightly brighter and situated only $3'$ from V 1162 Ori. Times of observations were recorded as mid–exposure and converted to Heliocentric Julian Date.

Using BV photometry obtained at SAAO and by photometry obtained at ESO (Paper I), we determined the relative colours of V 1162 Ori, the comparison star and a check star, GSC 4778–0025, which will be used to investigate the stability of the comparison star. The V, $B-V$ values for V 1162 Ori were fixed to those of Poretti et al. (1990, $V = 9.89$, $B-V = 0.31$), and $b-y$ to that of Hintz et al. (1998, $b-y = 0.187$). We found that the comparison star, GSC 4778–0019 ($V = 9.73$, $B-V = 1.55$, $b-y = 0.91$) is very red, and differs significantly in colour from V 1162 Ori. The check star, GSC 4778–0025 ($V = 12.58$, $B-V = 0.80$, $b-y = 0.47$), is somewhat fainter than V 1162 Ori and the comparison star.

Photometric light curves of very different length and quality were collected at the many sites during the campaign. As noted above, some light curves cover only single maxima or minima, while others cover several hours and cycles. The observations were not coordinated, but in a few cases did observations overlap, unfortunately only shortly and in poor weather at one or both sites. In Fig. 1 we show examples of overlapping data from two nights during which the weather was non–photometric at one of the two sites. The agreement between the overlapping data is fairly good. We show the difference between the data from the two sites (triangles); the scatter is high in the first night (7.4 mmag rms) and at a more acceptable level during the second night (4.8 mmag rms). In the left–hand panel there is also a systematic trend present in the difference. Such trends can be due to differences in filter passbands or, because the comparison star is very red, extinction. Our best PMT data have rms–scatter within a night of just below 2 mmag, whereas our best CCD data have rms scatter of about 2.5 mmag.

3. Frequency analysis

The frequency analysis was carried out using the excellent Fourier analysis tool Period98 (Sperl 1998). Amplitudes are in the following given as half the peak–to–peak value, and as criterion for detection of a pulsational frequency we require the corresponding peak in the amplitude spectrum to have an amplitude of at least 4 times the average noise, determined after prewhitening, in the frequency domain where it is found (Breger et al. 1993). This requirement can be lowered to 3.5 for combination frequencies as they occur at known positions (Breger et al. 1999).

3.1. Low–frequency analysis and stability of the comparison star

The stability of the comparison star, GSC 4778–0019, was investigated using CCD observations also including the

Table 1. List of sites participating in the campaign. Telescope diameters are given in meters.

Observatory	Location	Observer (#extrema)	Telescope	Detector	#hours
SAAO	S. Africa	T. Arentoft (44), L. Freyhammer (30), G. Handler (16)	1.00	CCD	77.0
SAAO	S. Africa	G. Handler (6)	0.75	PMT	4.9
SAAO	S. Africa	G. Handler (6)	0.50	PMT	3.1
Athens University	Greece	P. Niarchos, K. Gazeas, V. Manimanis (26)	0.40	CCD	33.2
Kryonerion	Greece	P. Niarchos, K. Gazeas, V. Manimanis (17)	1.22	CCD	22.9
LNA	Brazil	A. Bruch (26)	0.60	CCD	33.5
Xinglong	China	Z. L. Liu, A. Y. Zhou, B. T. Du (16)	0.85	CCD	18.9
Beersel Hills	Belgium	P. Van Cauteren (14)	0.40	CCD	20.6
Ege University	Turkey	C. Akan, C. Ibanoglu, S. Evren, G. Tas (14)	0.48	PMT	25.5
San Pedro Martir	Mexico	E. Poretti (3)	1.50	CCD	3.8
Merate	Italy	E. Poretti (7)	0.50	PMT	10.8
Mt. Laguna	USA	D. W. Dawson (9), D. Johnson (2)	0.50	PMT	14.5
Siding Spring	Australia	R. R. Shobbrook (5)	0.61	PMT	6.2
Sierra Nevada	Spain	R. Garrido (4)	0.90	PMT	4.9
Braeside	USA	R. Fried (4)	0.40	CCD	4.6
ESO	Chile	C. Sterken (3)	1.54	CCD	4.3
Lick	USA	C. Blake (1)	1.00	CCD	1.4
Total		(253)			290.1

check star, GSC 4778–0025, on the frames. Of the campaign data we used for this purpose the extensive time–series data obtained at SAAO during 15 nights. We also used the CCD data obtained at ESO.

Low–frequency variations are clearly present in the SAAO V 1162 Ori data, giving rise to peaks in the amplitude spectrum of up to 8 mmag in the frequency range 0–2 d^{-1}, as shown in the upper panel of Fig. 2. The variations are also directly visible as shifts in the nightly zeropoints, especially after subtracting the main pulsation frequency at 12.7082 d^{-1}. The zeropoints of V 1162 Ori *minus* the comparison star were compared with those of the comparison star *minus* the check star. The sizes of the night–to–night changes in the former have values not systematically different from the changes in the latter, but with opposite signs, as is seen in the middle panel of Fig. 2. The nightly changes thus originate from the comparison star.

The cause of the variability in GSC 4478–0019 is unclear. It can be variable on a time scale of days or, as the star is very red, the night–to–night changes could be due to extinction effects. However, as the zeropoint shifts are very similar relative to two stars of different colour, V 1162 Ori and the check star, the variations cannot be ascribed to extinction. From the ESO data, we find the shifts to have the same size in the b and y filters. We calculated the amplitude spectra of the ESO 1998, ESO 1999 and new SAAO comparison *minus* check star data separately and searched for re–occuring peaks, but did not find any. The variations of the comparison star seem nonperiodic, or are not stable from year to year.

The difference between V 1162 Ori and the check star shows a much smaller degree of variation, although some datapoints in the lower panel of Fig. 2 deviate from the zero mean. However, the effects are small and could be caused by extinction. The corresponding amplitude spectrum, which is also shown in Fig. 2, has little power at low frequency. There are some ∼2 mmag peaks present near 0.9 d^{-1} (and 1 d^{-1} aliases), but similar peaks are not present in the corresponding ESO data. We do therefore not find evidence for the presence of low–frequency variations in V 1162 Ori.

We are mainly interested in the absence of signal in the frequency range 5–50 d^{-1} in the comparison star data, and using the SAAO CCD measurements of the comparison star relative to the check star, there are no outstanding peaks in this part of the amplitude spectrum. The amplitude spectrum, with a 4σ significance curve superimposed, is shown in Fig. 3. All peaks above 5 d^{-1} in frequency are statistically insignificant and can be considered noise peaks. If we combine the ESO and SAAO comparison star data, and correct for the changes in nightly zeropoint, the comparison star shows no periodic variability up to 0.7 mmag below 15 d^{-1}, and 0.5 mmag above (peak values). This is shown as the insert in Fig. 3. The amplitude spectrum was calculated up to 300 d^{-1} and no high–frequency periodic components were detected either. The individual light curves have typically a rms-scatter of about 4 mmag. The residuals after correcting for nightly zeropoint variations are, for both the ESO and SAAO data (and the combination of the two) normally distributed, and can be represented by Gaussians with values of σ of the expected 4 mmag.

3.2. Frequency analysis of V 1162 Ori

All data for which we could determine times of maximum or minimum light are included in the O–C

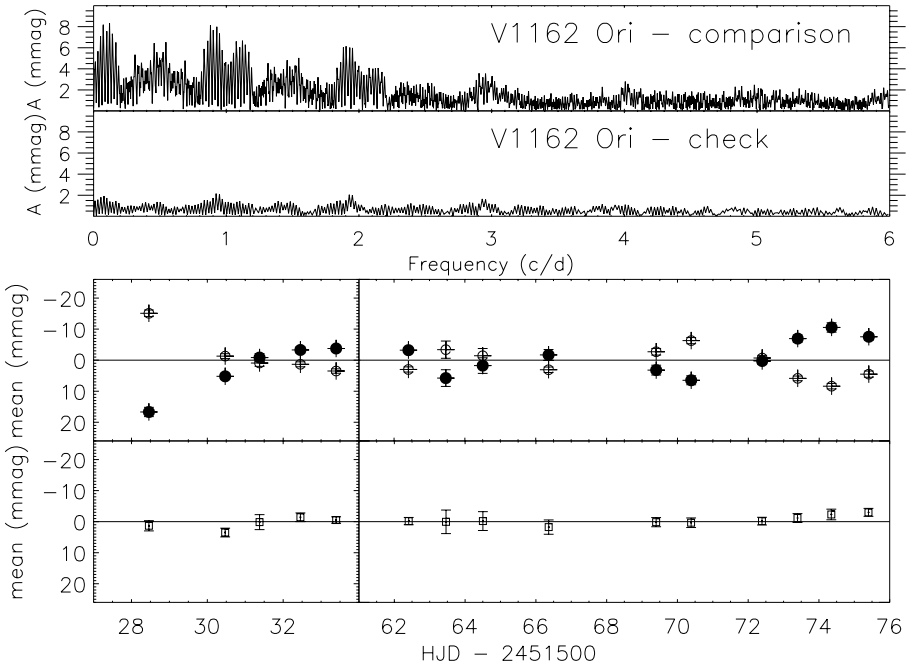

Fig. 2. Amplitude spectra in the low–frequency domain of V 1162 Ori (SAAO data, top). The lower panels show a comparison between the zeropoints in the differential light curves of V 1162 Ori *minus* comparison (filled circles), comparison *minus* check (open circles) and V 1162 Ori *minus* check (squares). The error bars are 3 times the error on each nightly mean value.

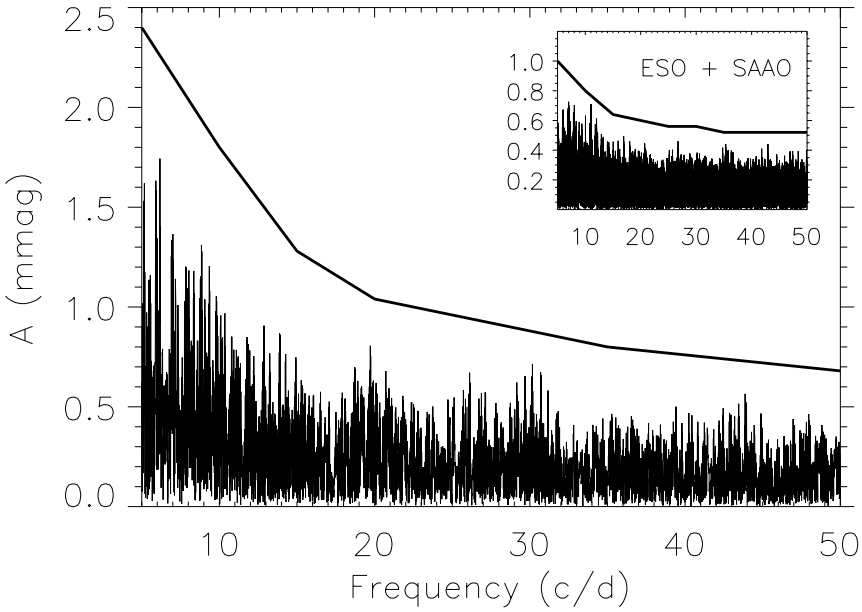

Fig. 3. Check for periodic variations of the comparison star in the frequency range where variations in V 1162 Ori are found. This diagram is based on the difference between the comparison star and the check star in the SAAO data. The solid line is a 4σ significance curve, found from local noise levels in the amplitude spectrum. The insert displays the amplitude spectrum of the ESO and SAAO data sets combined.

analysis in Sect. 4. For Fourier analysis of V 1162 Ori we selected, from the campaign data, long data strings covering more than one cycle and having well–defined zeropoints. Furthermore, only data obtained through the V–filter and of a sufficiently high quality were included.

Obvious bad points were removed from the data based on visual inspection of the light curves. In total, the data set for the Fourier analysis consists of 5388 datapoints, covering a time base of 134 days with an effective length of 139 hours of photometry obtained during 37 nights. 108 datapoints were rejected as being bad.

The data selected for Fourier analysis were then low–frequency filtered. This was done by zeropoint correcting data from the individual nights, and removing slow trends

by fitting 3rd degree polynomials to residuals from a provisional frequency solution and subtracting them from the original data. The filtering removes signals at low frequencies, up to about 5 d^{-1}. It was checked on the main pulsation at 12.7082 d^{-1} that frequencies in this area were not affected by the filtering: the amplitude and relative sizes of the side–lobes remained constant. This is expected as the frequency regions where peaks occur are well separated. However, the procedure has only marginal effect on the noise levels in the frequency regions under investigation here (5–50 d^{-1}), but we perform the filtering as we will later subdivide the data into smaller segments which will be more susceptible to effects of $1/f$–noise.

V 1162 Ori is known to display amplitude and period/phase variability on a relatively short time scale (Hintz et al. 1998; Paper I). We have to keep in mind the possibility that such changes occur within the time span of our data set, and if so, our analysis should take this into account. Such variability can lead to spurious peaks and/or increased noise levels in the residual amplitude spectrum (see e.g. Handler et al. 2000). Part of the latter could also be caused by filter passbands mismatches.

Using the filtered campaign data we first performed a regular frequency analysis of V 1162 Ori, not allowing for phase and amplitude variability. This was done to get an idea of the frequency content of the light curves before we include the earlier ESO data and allow the phase and amplitude of the main frequency to vary.

3.2.1. The campaign data

The amplitude spectrum of V 1162 Ori is dominated by the main periodicity at 12.7082 d^{-1} (f_1), but after prewhitening with this frequency, we detect the first two harmonics of f_1, and four additional frequencies on a statistically significant level. The successive (simultaneous) prewhitening of the amplitude spectrum is demonstrated in Fig. 4 and discussed below. The detected frequencies are marked with a square in each of the panels (a–f). The upper panel shows the original amplitude spectrum, and due to the high amplitude of f_1 it represents the spectral window function as well.

After removing f_1, the dominant set of peaks belongs to $2f_1$, and $3f_1$ is visible near 38 d^{-1} (panel b). Removing also the harmonics reveals several additional peaks in the residual amplitude spectrum (c). The highest of those occurs at 12.94 d^{-1}, i.e. close to, but clearly resolved from, f_1. However, to test the reality of this peak we subdivided the data in two nearly equal parts, and found it to be present in both, showing that this peak is not an artifact of f_1. Furthermore, the resolving power in each of the two subsets is, with time bases of 70 days, about 0.02 d^{-1} (Loumos & Deeming 1978), ten times higher than the separation between the two peaks in question. The 12.94 d^{-1} peak is also found in the SAAO data alone (and subsets thereof) and is thus not a spurious effect of merging data from several sites.

Gradual prewhitening by including the residual frequency of highest amplitude in the frequency solution (which is optimised after each additional frequency) allows us to detect the four low–amplitude frequencies. We label them f_2–f_5 and give the values of the frequencies, amplitudes and S/N in Table 3. *The tabulated values, however, are the solution from the combined ESO and campaign data set and will be discussed below.*

The choice of f_5 is not obvious (Fig. 4f), as three peaks have equal amplitude. We selected the central peak at 15.99 d^{-1}, but this peak may be an alias and not the true frequency. In the campaign data, the S/N is only 4.3, but it will be confirmed when we include the ESO data, as will a peak at 27.77 d^{-1} (g, marked position). This represents the first detection of multiple frequencies in V 1162 Ori.

We prewhitened the light curves for the 7 significant frequencies and calculated statistical weights, following Frandsen et al. (2001), from the residuals, to see if applying such weights could improve the noise levels. We also tried to decorrelate SAAO data residuals for effects of seeing, sky–background levels and relative position on the CCD chip, using the methods described by Frandsen et al. (1996, or see Arentoft et al. 2001). As neither of these two methods proved to have any effect on the noise in the investigated frequency region, we did not apply them to the data used in the further analysis. After subtracting the 7–frequency solution there are indications of additional peaks or increased noise levels in the 10−15 d^{-1} range of the amplitude spectrum, possibly originating at least partly from phase and amplitude variations of f_1. Dividing the data in smaller subsets suggested amplitude and phase variability of f_1 – the amplitude changes between 60 and 73 mmag during the campaign, and there is a drift in phase of about 30°. We will therefore take into account (A, ϕ)–variations of f_1 in the subsequent analysis. The reason why the residual amplitude spectrum displays relatively weak signal compared to the size of the amplitude variations is that, as will be shown below, the vast majority of the campaign data have nearly constant (high) amplitude – data with low amplitude constitute only a small fraction of the data set.

3.2.2. Including the 1998–1999 ESO data

At this point we also include the data obtained previously at ESO (Paper I) in the analysis, to seek confirmation of the newly detected low–amplitude frequencies in an independent data set, to expand our time base, and to use the combined data set to search for additional pulsation frequencies. The ESO data comprise about 111 hours of both b and y–photometry collected over 7 observing runs at ESO in early 1998 and 1999, and we add the y data to the 139 hours of V–photometry from the campaign data set. The pulsation amplitude was found to be similar in the V and y filters in Paper I, but varied from about 60 to more than 75 mmag in y on a time scale of months. Furthermore, period changes were also present; including

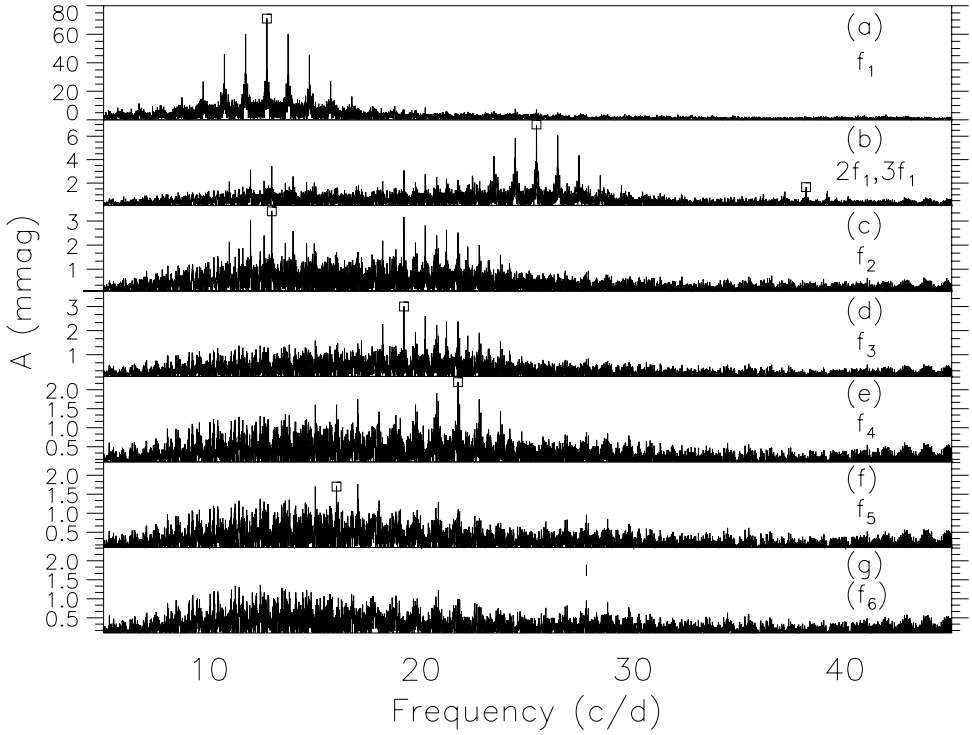

Fig. 4. Amplitude spectrum of V 1162 Ori with successive, simultaneous prewhitening of the detected frequencies (see text), using time–series data obtained during the campaign. Note that the low–amplitude frequencies, especially f_5 suffer from uncertainty due to aliasing.

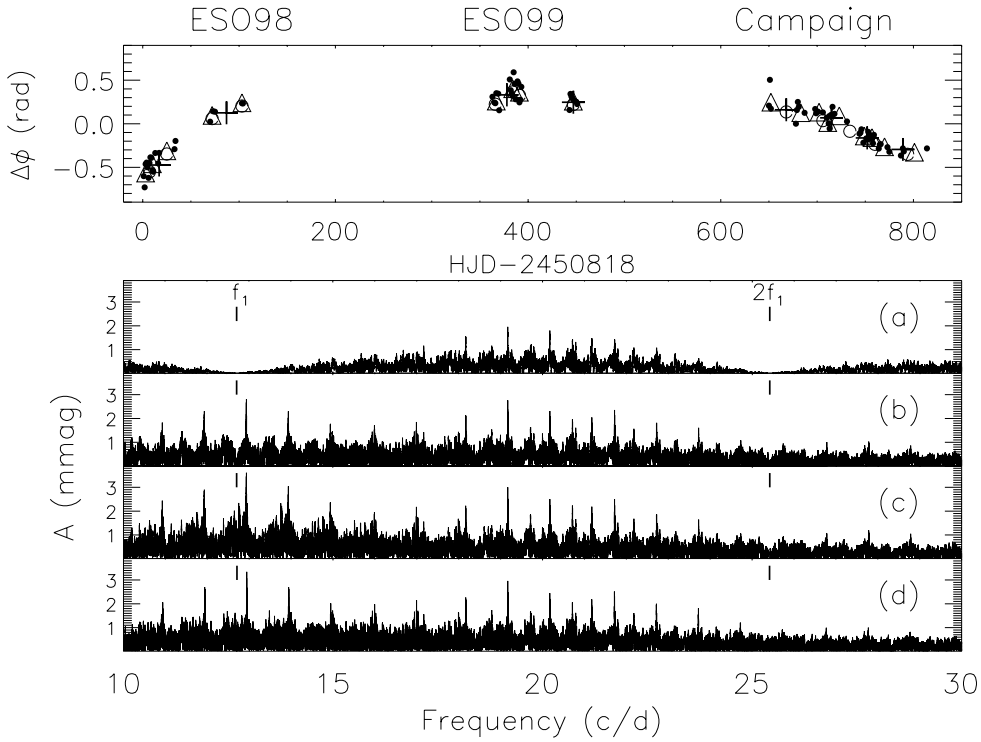

Fig. 5. The upper panel displays the evolution in phase of f_1 (12.708264 d^{-1}) determined from the four ways of dividing the data in subsets: **a)**–**d)** in Table 2. For error bars, see Sect. 3.3. The different parts of our data set are given above the figure. Dots are from **a)**, triangles from **b)**, open circles from **c)** and crosses from **d)**. The lower panel gives the residual amplitude spectrum for each of the cases **a)**–**d)** after removing $f_1$and its harmonics, taking (A, ϕ)–variations into account (see text). The position of f_1 and $2f_1$ has been marked in the amplitude spectra. The 2.2 mmag peak close to f_1 in **c)** is not a remnance of f_1 but a close–by noise peak.

those data in the analysis requires that we take (A, ϕ)–variations into account. We also include an additional 10 hours (335 datapoints) of mainly short light curves obtained during the campaign, which were not included in the Fourier analysis above. They will increase the time resolution in the investigation of (A, ϕ)–variations.

To be able to take (A, ϕ)–variations of f_1 into account, we need to subdivide the dataset into smaller subsets to allow fitting of f_1 and $2f_1$ within each subset. The subsets should, when possible, have a time base sufficiently long for the individual frequencies to be resolved, but not so long that possible variations are undersampled. In short, our final results must not depend on the choice of subsets. We tested four different ways of subdividing the data: (a) treating each night individually, (b) using 18 subsets of 2–8 nights of data (2 nights only in cases of isolated data), (c) 13 subsets of slightly longer time base, or (d) 8 subsets combined of 2–3 of the subsets in (b). We will refer to the labels a–d below.

The four sets are outlined in Table 2[1]. In each case we performed a preliminary frequency analysis allowing for (A, ϕ)–variations. We fixed f_1 to the optimal frequency, 12.708264 d^{-1}, determined from a fit to the combined data set, and left the amplitude and phase of f_1 and $2f_1$ as free parameters within each subset. The residual amplitude spectra after subtracting f_1 and $2f_1$ are displayed in Fig. 5, lower half. Subdivision (a) leads to overfitting of the data, which is seen as a suppression in the noise level around f_1 and $2f_1$ – this is an artifact of fitting with too many degrees of freedom. (b) gives reasonable results, but there is a small dip in the noise level at f_1, and the amplitude of the close–by peak at 12.94 d^{-1} is slightly lower than in (c) and (d), which gives similar results for the amplitudes of the low–amplitude modes. The noise level in the region 10–20 d^{-1} of the residual spectra is slightly lower in case (d), also after prewhitening with the low–amplitude frequencies detected above. However, (d) has the disadvantage of the (A, ϕ)–variations being poorly sampled, and for investigating such variations we will use subdivisions (b) and (c) to obtain higher temporal resolution.

In searching for low–amplitude frequencies we are interested in as low a noise as possible, and subdivision (d) will therefore be used for this analysis. The results of the frequency analysis should not differ between (c) and (d), and we can use (c) as control, thus minimising the risk of detecting spurious peaks. In the four cases we can determine the evolution of the phase of f_1 in time as seen in Fig. 5, upper panel, which has the same shape regardless of choice of subset sizes. This figure shows that (A, ϕ)–variations of f_1 must be taken into account in the analysis. f_1 is by far the dominant frequency, which is why even fitting within the individual nights gives reasonable values for the phases, despite poor frequency resolution.

If (A, ϕ)–variations are disregarded when subtracting f_1 there remains a residual signal in the amplitude spectrum near f_1 (at 12.71197 d^{-1}) of 13 mmag and near $2f_1$, at (f_1+ 12.71197 d^{-1}), of 2 mmag. The peak close to f_1 may be a real peak, or a result of amplitude and phase variability of f_1. In the latter case is a peak at the sum–frequency also expected, as $2f_1$ will be modulated in the same way as f_1. Such close (real) peaks would cause amplitude and phase variability through beating, and to test their reality, we included them in the frequency solution instead of allowing f_1 to vary. This resulted in a 30% higher noise level, indicating that they are indeed not real frequencies. Another way of testing their reality is, following Handler et al. (2000), to compare the amplitude ratio of f_1 and $2f_1$ to their close-by peaks. These ratios should differ if the frequencies are real and the pulse shapes of the individual signals should not vary. The ratios differ, but our data may not be sufficient to allow a reliable determination. Consequently, we leave these peaks close to f_1 and $2f_1$ out of our frequency solution, but will return to them in the discussion.

3.2.3. The combined ESO and campaign data set

The combined ESO y and campaign data set consists of 7552 datapoints spanning a time base of 815 d. We successively subtracted the frequencies detected in Sect. 3.2.1, allowing for (A, ϕ)–variations of f_1 and its harmonics using subdivision (d). It was verified that these frequencies were present in the combined data set as well, with f_2 and f_3 as the dominant peaks in the spectrum after subtracting f_1. The residual spectrum after subtracting f_1 and its harmonics can be seen in Fig. 5, bottom panel. The alias ambiguity in the determination of f_5 is not cleared by the combined data set.

We then searched for additional significant peaks. The peak at 27.77 d^{-1} is statistically significant in the combined amplitude spectrum, as tabulated in Table 3. This peak has the same amplitude, when using subdivision (c), but its presence may be uncertain due to the very low amplitude. Its likely presence is displayed in Fig. 6. No further frequencies were found, and we note that f_1 is the lowest frequency of the detected modes.

The ESO light curves covered only 1–3 hours per night, resulting in a poor spectral window function. After removing f_1 and $2f_1$, allowing for (A, ϕ)–variations, the residual amplitude spectrum of the ESO data set alone can be seen in Fig. 7. The above detected low–amplitude frequencies are also present in the ESO data set, and are thus confirmed as they are found in two independent data sets.

3.3. Amplitude and phase variations

We will now seek to characterise in detail the (A, ϕ)–variations taking place in f_1, and furthermore search for variability of the low–amplitude frequencies. The procedures described in this section are largely based on the methods used by Handler et al. (2000) in their analysis of XX Pyx. We keep in mind that these authors, using a

[1] Available at CDS.

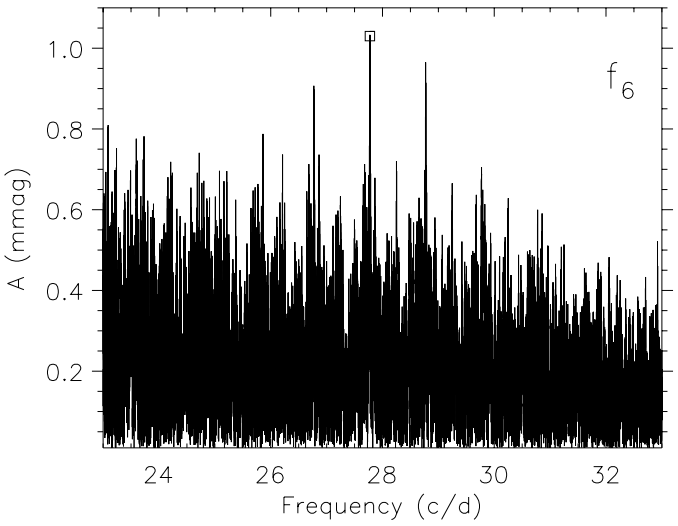

Fig. 6. The new probable frequency (f_6) detected from the combined data set. The position of the frequency is marked with a square.

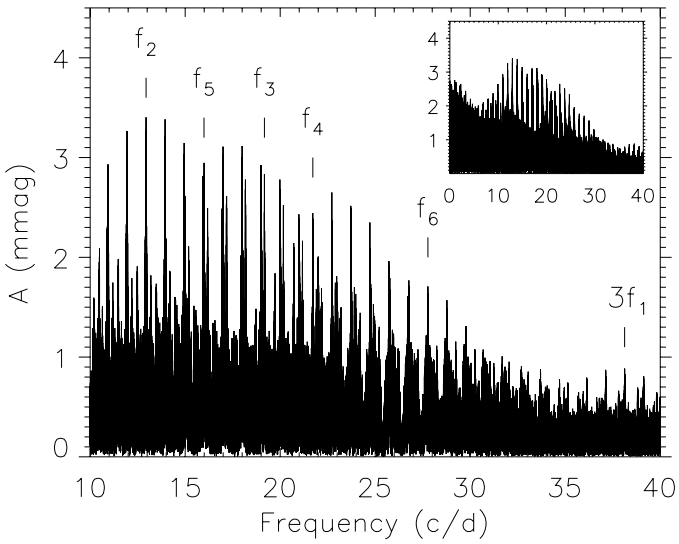

Fig. 7. Residual amplitude spectrum of the ESO 1998–99 data, after prewhitening with f_1 and $2f_1$. The position of the low–amplitude frequencies detected from the combined data set are indicated. The insert shows also the low–frequency part of the amplitude spectrum.

Table 3. Table of detected frequencies in V 1162 Ori , from the combined data (campaign and ESO 1998–1999). The amplitudes of f_1 and its harmonics are average values, as we have allowed for amplitude and phase variations. Overall residual scatter after subtracting this frequency solution is 6.2 mmag. The last column gives the frequency ratio (f_1/f_n), discussed in Sect. 3.4.

ID	Frequency (d^{-1})	Amplitude (mmag)	S/N	f_1/f_n
f_1	12.7082	66.6	151	1.000
$2f_1$	25.4164	6.6	27	–
$3f_1$	38.1246	1.3	8	–
f_2	12.9412	3.2	7	0.982
f_3	19.1701	3.0	9	0.663
f_4	21.7186	2.4	8	0.585
f_5	15.9901	2.1	5.5	0.795
f_6	27.7744	1.1	5	0.458

larger data set, did not consider phase variability of modes with amplitudes lower than 1.5 mmag, as the phases of those modes were not sufficiently constrained.

Before we start the analysis we will address the question of error bars on the amplitude and phase values. We calculated these following Montgomery & O'Donoghue (1999). However, the formal error bars are unrealistically small, as was also discussed by Handler et al. (2000) who found the error calculations to be underestimated by a factor of two or more. In our data we would expect residual noise levels in the amplitude spectrum of less than 0.1 mmag (assuming white noise). The residual noise levels were 0.4 mmag at 15 d^{-1} and 0.16 mmag at 38 d^{-1}. In the following we therefore multiply the formal errors by a factor of two to obtain more realistic, but possibly still underestimated, error estimates.

3.3.1. f_1

We used the combined data set prewhitened for the low–amplitude frequencies to investigate (A, ϕ)–variations of f_1. To subtract the low–amplitude frequencies we first subtracted f_1 and its harmonics, allowing for (A, ϕ)–variations using subdivision (d). This led to a time string whose amplitude spectrum displayed only noise at f_1, $2f_1$ and $3f_1$. Having removed the influence of f_1, f_2 – f_6 were then fitted to the residuals, creating a synthetic time string which was subtracted from the original data. It was checked that this method removed the low–amplitude frequencies well.

Because we used a data set prewhitened for the low–amplitude modes, and as a result of Fig. 5, upper panel (showing that the choice of subset sizes does not influence the shape of the phase variations), we used the 18 subsets of subdivision (b) for the investigation of (A, ϕ)–variations of f_1, as we are interested in a high time resolution.

We show the evolution in amplitude of f_1 in Fig. 8. Very large variations are present, and they appear cyclic. We have superimposed a sinewave with a period of 282 ± 6 d, which seems to describe the amplitude variations of both f_1 and $2f_1$ well, although the scatter in the bottom panel is high and the agreement with the fit only suggestive. Especially the data from March 1999 (at 460 d) show a very high amplitude value of $2f_1$. The amplitudes of the sinewaves are 9.85 mmag for f_1 and 1.7 mmag for $2f_1$, with average values of 64.36 and 5.98 mmag, respectively. The parameters of the fit were determined by least–squares fitting to the (only) 18 f_1 data points, and residual scatter is 1.47 mmag for f_1 and 0.90 mmag for $2f_1$, lower than the scatter in the individual data subsets.

Figure 8 also shows that a large fraction of the campaign data have nearly constant amplitude (over 70 mmag), as mentioned in Sect. 3.2.1. There is a larger scatter around the last maxima in the upper panel of Fig. 8 (f_1), where the fit deviates up to 2 mmag from the datapoints. This may be due to the presence of additional effects, and the reason it is seen being the larger amount of data available. Another explanation may be that the error bars still underestimate the real scatter. To test the reality we determined the amplitude with smaller and larger subsets, but the same shape remained. Regardless, the suggested cyclic variation cannot explain the amplitude variations observed prior to the ESO data, as Lampens (1985) found an amplitude of 92 mmag, Poretti et al. (1990) derived one of 98 mmag, and Hintz et al. (1998) found amplitudes of 72 and 50 mmag from two different data sets – three of these four measurements are thus outside the amplitude range of the upper panel of Fig. 8. We note that the shape of the amplitude variations does not change when using the original, non–prewhitened data instead. Given the cyclic shape of the amplitude variations it is not surprising that a peak is present in the amplitude spectrum very close to f_1 (Sect. 3.2.2). The beat period of f_1 and the close peak is about 270 d, consistent with the time scale of the cyclic variation in amplitude.

The shape of the phase variations of f_1 in Fig. 9 is the same as in Fig. 5, showing that the low–amplitude modes do not influence the phase determinations – they have been prewhitened in Fig. 9 but not in Fig. 5. Phase changes are clearly present, both in f_1 and in $2f_1$. The shape of the phase changes appears parabolic, or, as the maximum is very broad, possibly piecewise linear. This will be discussed in detail in Sect. 4.

The amplitude and phase variations are not directly correlated, which is especially seen from the high amplitude of the datapoints from March 1999. We have in Fig. 9 superimposed the suggested sinewave from the amplitude variations, but with different values for phase and amplitude. There is reasonable agreement with the curve for the phases of the ESO data (before HJD 2451300), but not for the phases of the campaign data. The descending branch seen in the latter is less steep than expected from the fit, and the overall shape is clearly not purely sinusoidal. Thus simple beating between two close frequencies alone cannot describe the observed variations.

As the (A, ϕ)–variations are clearly present in the ESO data, which were all taken using the same instrumental setup, the variations in amplitude are not caused by spurious effects of data merging or from filter passband mismatches between individual sites.

There are several mechanisms which could cause variations in the light curve shape of a pulsating variable, e.g. a beat phenomenon, where the pulse shape will vary according to the beat phase (Poretti 2000). Consequently we calculated, within the subsets, the phase difference (ϕ_{21}) and the amplitude ratio (R_{21}) of f_1 and $2f_1$. The results are shown in Fig. 10 as a function of time (upper panels) and of the amplitude of f_1 (lower panels). The straight line in the bottom panel is a weighted linear fit to the data.

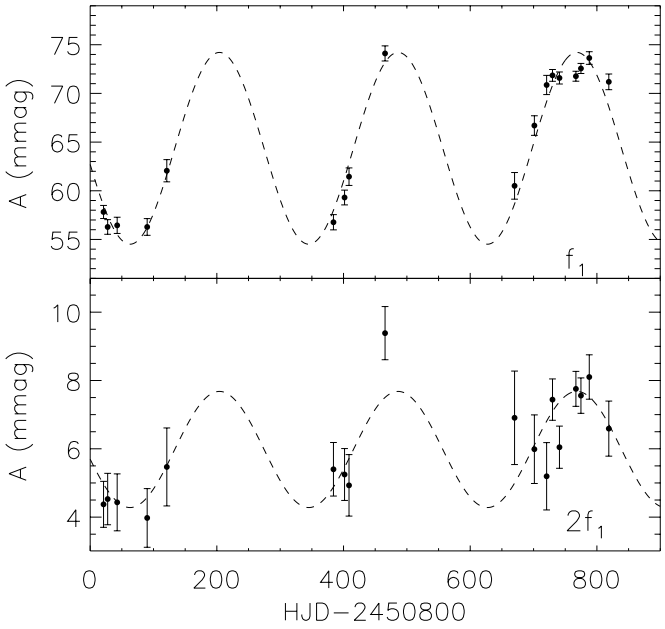

Fig. 8. Variation in amplitude of f_1 (top) and of $2f_1$ (bottom). The variations appear sinusoidal, and are present in both f_1 and $2f_1$. Error bars are discussed in the text. The dashed curves are sinewaves found from an optimised fit to the amplitude values of f_1 with scaled amplitude for $2f_1$.

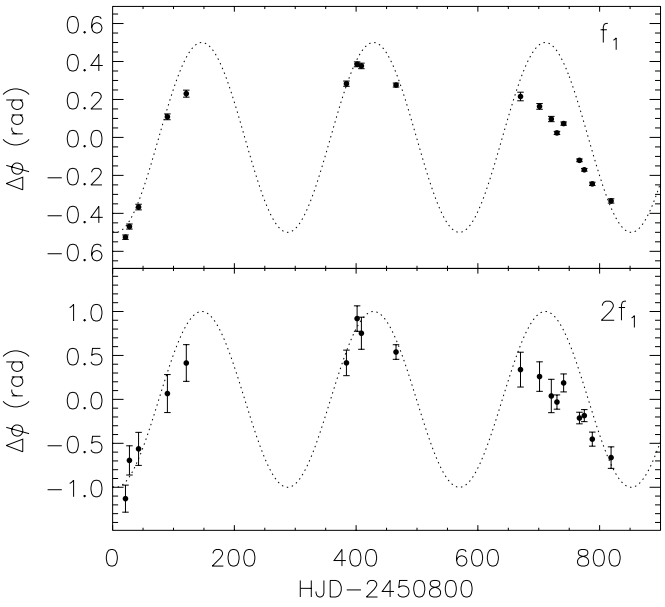

Fig. 9. Variation in phase of f_1 (top) and of $2f_1$ (bottom). A sinewave with the period deduced from the amplitude variations is superimposed.

The figure shows that the phase difference between f_1 and $2f_1$ remains constant both as a function of time and f_1–amplitude, whereas the amplitude ratio (R_{21}) may grow with larger amplitude of f_1. The slope of the fit to R_{21} vs. A_{f_1} is 0.0015 ± 0.0004, thus formally significant, but the fit does not appear fully convincing to us.

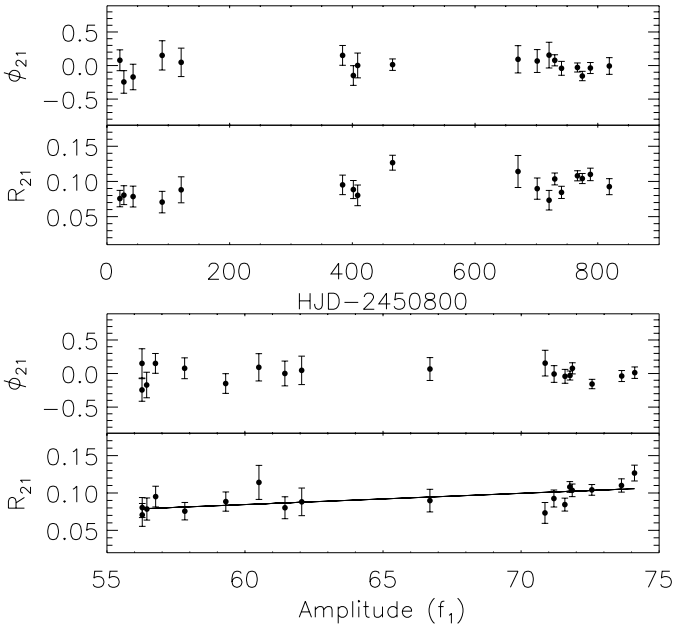

Fig. 10. Effects of the amplitude and phase variations on the pulse shape, as a function of time (top) and amplitude of f_1 (bottom). Whereas the phase difference ($\Delta\phi = 2\phi_{f_1} - \phi_{2f_1}$) is constant, this appears not to be the case for the amplitude ratio (A_{2f_1}/A_{f_1}, see text).

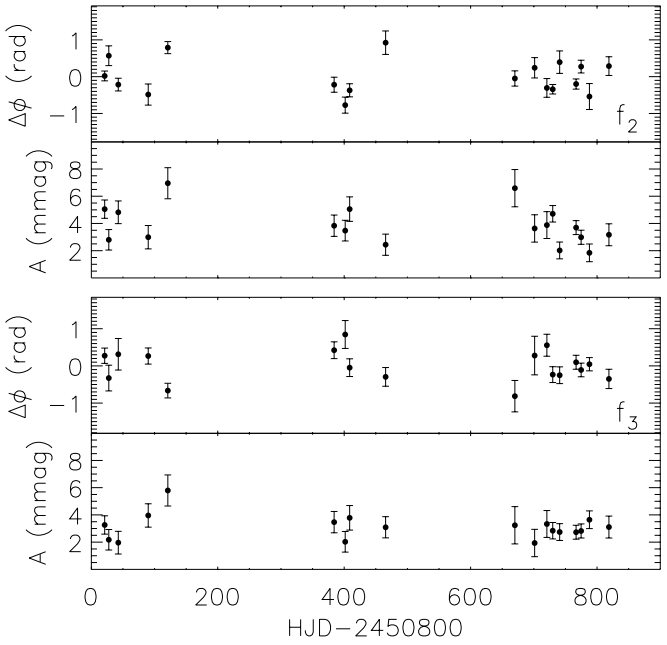

Fig. 11. Phase and amplitude of f_2 and f_3 as function of time.

Furthermore, as A_{2f_1} is expected to scale with $A_{f_1}^2$ (see Garrido & Rodriguez 1996 and references therein) such a variation is not surprising; $A_{2f_1}/A_{f_1}^2$ does not correlate with A_{f_1} (not shown). In any case, the variation appears uncorrelated with the trend of ϕ_{21} vs. A_{f_1}. This suggests that the pulse shape of f_1 remains nearly constant during the amplitude variation, supporting an intrinsic amplitude variation rather than a beat phenomenon.

3.3.2. Low–amplitude frequencies

We used the combined data set prewhitened for f_1 and harmonics to investigate possible variability of the low–amplitude modes. The five low–amplitude frequencies were optimised to the complete data set and fixed. The amplitudes and phases were then optimised while allowing one frequency at a time to have variable amplitude and phase. This gave, for each frequency, a set of amplitudes and phases as a function of time. For each frequency we then created "single–mode data sets", as in Handler et al. (2000), by subtracting from the light curves all the other frequencies but the one under investigation. This was done using a $(n-1)$ simultaneous fit to the data.

We tried different ways of subdividing the data (b,c), but only for f_2 and f_3, the strongest of the low–amplitude signals, were meaningful results obtained – i.e. only for these two frequencies were the results independent of the method used. The results are displayed in Fig. 11. The scatter in this plot is quite high, and although trends or deviations from point to point in some cases are present, Fig. 11 does not show convincing evidence for (A, ϕ)–variations of the low–amplitude modes. The amplitude modulation present in f_1 does not seem to be present in the low–amplitude modes, only the first amplitude values (from the 1998 ESO data) have a shape similar to that of f_1.

3.4. Colour photometry

From the ESO data we determined the average difference between the times of minimum and maximum light in the b and y filters. This difference ($T_{\mathrm{ext},b} - T_{\mathrm{ext},y}$) amounts to -0.00010 ± 0.00007 d, or a phase shift between b and y of $+0\overset{\circ}{.}5 \pm 0\overset{\circ}{.}3$. From the light curves themselves we find a phase shift for f_1 of $+0\overset{\circ}{.}75 \pm 0\overset{\circ}{.}4$ between b and y, with the error estimate again scaled by a factor of two.

Using $uvby\beta$ photometry and physical parameters from Hintz et al. (1998) we verified that V 1162 Ori is well placed in the HADS instability strip (McNamara 2000). Using the Moon & Dworetsky (1985) code we found a $T_{\mathrm{eff}} = 7400$ K and $M_V = 1.89$, in agreement with Hintz et al. (1998).

We then determined from our own data a f_1 phase difference $\phi_{b-y} - \phi_y = +5^\circ \pm 2^\circ$, and an amplitude ratio $A_{b-y}/A_y = 0.23 \pm 0.02$. The values agree well between two subsets of the data (1998 and 1999, separately). The colour data are not sufficiently abundant to allow meaningful determination of phase shifts for the low–amplitude frequencies.

In Fig. 12 we compare these values for f_1 with theoretical predictions (Garrido et al. 1990; Garrido 2000). Model atmospheres were calculated assuming Pop I, $T_{\mathrm{eff}} = 7400$ K, $\log g = 3.96$ (Hintz et al. 1998) and $\alpha = 1.25$. For Q we used the calibration given in Breger & Pamyatnykh (1998), and found $Q = 0.029$ d assuming a mass of 1.8 $M_\odot$

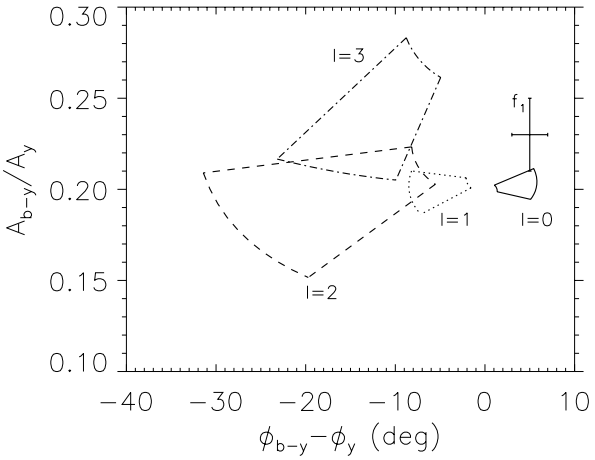

Fig. 12. *Regions of interest* for V 1162 Ori, pointing to f_1 being radial. See text for discussion.

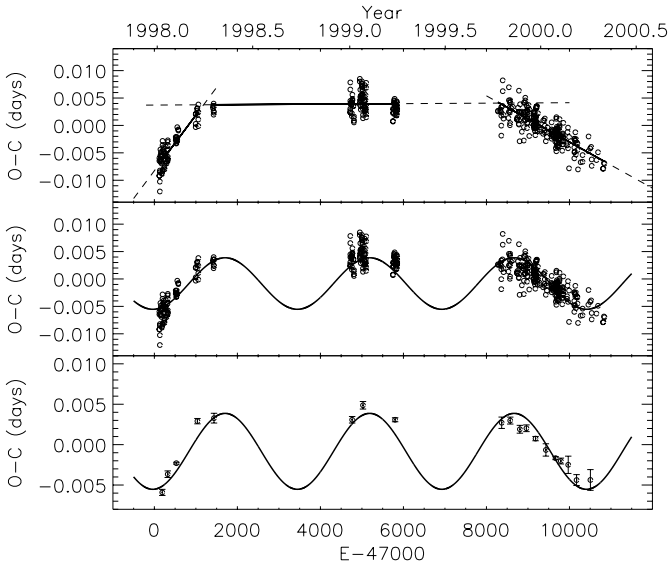

Fig. 13. O–C diagrams for times of maximum and minimum light in the combined data. The superimposed solutions are piecewise constant periods (upper panel) and a sinewave (middle panel). The latter is repeated with binned data (on a larger scale) in the lower panel. The error bars show the errors on the mean values of the bins. P_0 is 0.07868895 d, corresponding to the frequency of f_1 found in Sect. 3.2.2.

(Hintz et al. 1998) and a bolometric correction of $-0\overset{\mathrm{m}}{.}1$. The positive phase shift indicates a radial f_1. The deviation from the predicted amplitude ratio is likely due to the present accuracy of the model atmospheres (see e.g. Garrido 2000), which are furthermore highly temperature dependent.

The error associated with Q is too large to distinguish between the fundamental mode ($Q = 0.033$) and the first overtone ($Q = 0.026$). However, the dominant frequency in HADS is expected to be the fundamental (e.g. McNamara 2000).

The last column of Table 3 gives the frequency ratios relative to f_1. For δ Scuti stars a ratio of fundamental to first overtone of 0.77–0.78 is expected (see e.g. Petersen & Christensen–Dalsgaard 1996), which is not found for any of the low–amplitude frequencies. Furthermore, they do not show a regular frequency spacing with f_1, and most of them are very likely non–radial. Especially f_2 is too close to f_1 for both of them to be radial.

4. O–C analysis

Following Sterken et al. (1987), the times of maximum and minimum light were determined by fitting 3rd degree polynomials to the extrema in the light curves. During the campaign, eleven extrema were measured at two sites simultaneously, which offers another order–of–magnitude estimate of the precision in the timings. The simultaneous measurements deviated mutually with a mean of 0.0009 d (0.0005 d median), and they provide a realistic uncertainty estimate of the timings. The extrema collected during the campaign are presented in Table 4, the earlier ESO–extrema are published in Paper I.

The O–C diagrams are displayed in Fig. 13, which includes times of maximum as well as minimum light. A constant O–C shift between the maxima and minima of 0.0027 ± 0.0004 d (caused by the non–sinusoidal shape of the light curve of f_1) was found and corrected for. This corresponds to a positive shift of the minima in pulsational phase of f_1 of 0.03 ± 0.01 cycles, similar to what was found in Paper I. This asymmetry is a general feature of HADS (McNamara 2000). To check whether deviations from regularity in the light curve shape, (e.g. from a changing pulse shape) could influence our results, we also performed the analysis on the maxima and minima separately. The results were found to agree.

The shapes in the O–C diagrams correspond to the shape of the phase variations in Fig. 9, as one would expect – the two diagrams are equivalent. In Fig. 13 we show two possible fits to the data, piecewise linear segments (period breaks), and an optimised sinewave with a period very similar to that of the amplitude variations. The best of these solutions is the piecewise linear fit which leaves residual O–C scatter of 0.0016 d, while the sinewave leaves a scatter of 0.0020 d. This is not unexpected as the piecewise linear fits have more degrees of freedom. In the lower panel of Fig. 13, the data have been binned in smaller segments. The binned O–C values show overall deviations from a sinewave fit larger than the error bars. The campaign datapoints are systematically below the fitted curve at maximum, and above at minimum.

Our data only cover a relatively short time base in terms of O–C patterns, and may sample only a small part of a large scale structure. We therefore include the extrema published by Hintz et al. (1998) in the analysis, as shown in Fig. 14, upper panel. The overall shape of this diagram is parabolic, but with additional effects present. A parabolic fit with a linear period change rate of -5×10^{-9} s s^{-1} (calculated as described by e.g. Sterken 2000) is subtracted in the middle and lower panels. The residuals can now to some extent be described by a

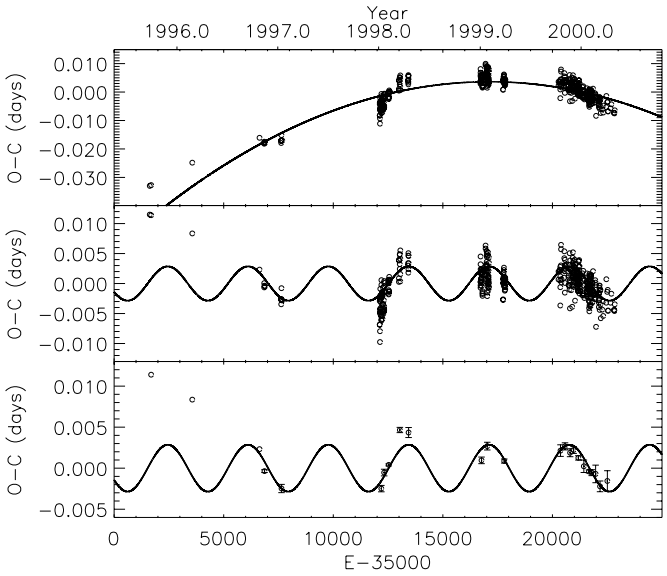

Fig. 14. O–C diagrams for our times of maximum and minimum light combined with the times of maximum published by Hintz et al. (1998). Upper panel: large scale variations can be described by a parabola. Middle panel: subtracting the parabolic shape leaves residuals which, except for the first datapoints, may possibly be described by a sinewave with a period of 285 d and an O–C amplitude of 0.0029 d. In the lower panel have the data been binned (shown on a larger scale). P_0 is 0.07868910 d.

sinewave, but several points still deviate by several σ, and they may be better described by piecewise linear segments. The same is the case for the phase values in Fig. 9: the residuals after correcting for a linear phase change still deviates from a sinusoidal shape (not shown). The superimposed sinewave has a period of 285 ± 3 d, in agreement with the time scale of the amplitude variations (282 ± 6 d).

If a cyclic variation is present in the O–C diagram, the time scale is thus the same as for the amplitude modulation. The fact that these match is an argument that the variations in the O–C diagram are indeed cyclic – except if the phenomenon causing the amplitude variations also causes the main period to change abruptly on the same time scale. In any case, the first datapoints in Fig. 14 are not described by a cyclicly changing period (unless the overall shape in the upper panel is not parabolic, but rather sinusoidal with a very long period), and neither are the data from Poretti et al. (1990): a model of a slow linear change with a cyclic component superimposed cannot fit the data completely. For the binned data, subtracting four piecewise linear segments (in Fig. 14: $E < 10\,000$, $10\,000 < E < 15\,000$, $15\,000 < E < 21\,000$ and $E > 21\,000$) leaves a residual scatter of 0.0007 d. Subtracting a sinewave leaves one of 0.0010 d, and in both cases the residuals vs. epoch leaves no trend.

Subtracting the sinewave before performing the parabolic fit (and excluding the first datapoints) yields a linear period change rate of -5.1×10^{-9} s s^{-1}, or a value of $(1/P)(\mathrm{d}p/\mathrm{d}t) \sim -2.4 \times 10^{-5}$ yr^{-1}. This is a very high rate of change, and only expected for pre-main sequence or very evolved stars (Breger & Pamyatnykh 1998) – and with opposite sign of what is expected for the majority of δ Scuti stars.

The residual scatter in the non–binned O–C diagram, is, after subtracting parabolic and cyclic variations (or piecewise linear segments) 0.0018 d. This is a factor of two larger than what is expected from our measurements of the precision on the individual timings (0.0009 d). As the cause of this could be the multiperiodicity of V 1162 Ori, we re–determined the extrema from the data set prewhitened with the low–amplitude frequencies, but found the same scatter to be present. This type of enhanced scatter may be an intrinsic feature in HADS (Szeidl 2000).

5. Discussion and conclusions

Several very interesting phenomena are present in the light curves of V 1162 Ori, including multiperiodicity and cyclic amplitude variability. The O–C analysis reveals the presence of a linear period change whose size is too large to be reconciled with evolutionary changes as given by Breger & Pamyatnykh (1998). However, these authors have collected available information on observed period changes in δ Scuti stars and find that the observed values, which are distributed nearly evenly between increasing and decreasing periods, disagree with stellar evolution calculations. They conclude that the observed linear period changes are not caused by evolutionary effects, but rather by long–period binarity or nonlinear mode interactions.

On top of the linear change are O–C variations which can be explained by frequent period changes or a cyclic variation combined with sudden changes. In both cases is the time scale of the period variation similar to that of the amplitude modulation, making a common origin probable.

Cyclic variations in the O–C diagram are explained either by the light time effect caused by the motion of the pulsating star in a binary system, or by beating of two (or more) very closely–spaced frequencies. These possibilities were put forward for V 1162 Ori already in Paper I. In Sect. 3.2.2 we noticed a peak in the amplitude spectrum very close to f_1, but considering the *nearly* cyclic amplitude and phase variations present in the data, such a close peak would always be expected, as discussed in Sect. 3.3.1.

Including this close peak in the frequency solution still leads to an increased noise level in the residual amplitude spectrum of 15% even if we take the linear variation in period of f_1 into account. Furthermore, with a pure beat of f_1 with a single close frequency, we cannot explain the deviations from a sinusoidal shape in the O–C diagram corrected for the linear period change (Fig. 14, middle and lower panels). A linear change combined with beating between two close frequencies is therefore, based on the present data, not a likely (or at least not the only) explanation of the observed changes.

Table 4. New times of maximum and minimum light (HJD−2450000). The error on the time is estimated to be 0.0009 d. The cycle count scheme is based on Hintz et al. (1998).

$T_{\max}$	E	$T_{\max}$	E	$T_{\max}$	E	$T_{\min}$	E	$T_{\min}$	E	$T_{\min}$	E
1460.5794	55279	1528.4862	56142	1573.4161	56713	1460.6223	55279	1539.7801	56285	1606.3490	57131
1464.5925	55330	1528.5654	56143	1573.4942	56714	1466.9130	55359	1546.2318	56367	1607.2947	57143
1465.5370	55342	1528.5654	56143	1574.2797	56724	1466.9959	55360	1548.4375	56395	1608.3136	57156
1466.7965	55358	1528.6426	56144	1574.3571	56725	1469.5985	55393	1549.3013	56406	1611.3046	57194
1466.8718	55359	1528.7222	56145	1575.3043	56737	1471.0086	55411	1549.3796	56407	1620.9812	57317
1466.9523	55360	1528.7995	56146	1575.3812	56738	1481.3219	55542	1553.3919	56458	1631.9209	57456
1469.0000	55386	1530.3744	56166	1575.4601	56739	1483.2822	55567	1562.2839	56571	1638.2145	57536
1469.6322	55394	1530.4536	56167	1576.3249	56750	1483.3650	55568	1562.3629	56572	1661.4271	57831
1471.0436	55412	1530.5302	56168	1576.4041	56751	1483.6802	55572	1562.4420	56573		
1480.3290	55530	1531.3188	56178	1577.0364	56759	1496.5817	55736	1562.5207	56574		
1481.1957	55541	1531.3950	56179	1577.2705	56762	1497.2898	55745	1564.4883	56599		
1481.2765	55542	1532.3416	56191	1577.3507	56763	1499.9645	55779	1566.3755	56623		
1483.2425	55567	1532.4205	56192	1577.3509	56763	1500.2799	55783	1569.3649	56661		
1483.3202	55568	1532.4990	56193	1578.2935	56775	1500.3640	55784	1570.3080	56673		
1483.4008	55569	1532.5803	56194	1582.3065	56826	1500.9890	55792	1570.4677	56675		
1483.6330	55572	1533.2851	56203	1582.3826	56827	1501.6138	55800	1571.2517	56685		
1483.7140	55573	1533.3672	56204	1583.2500	56838	1505.9471	55855	1571.3345	56686		
1485.5243	55596	1533.4444	56205	1583.4087	56840	1509.6402	55902	1571.3366	56686		
1488.5147	55634	1533.5217	56206	1584.2723	56851	1509.7258	55903	1571.4150	56687		
1496.6174	55737	1534.4690	56218	1584.3515	56852	1512.3995	55937	1571.8035	56692		
1497.2472	55745	1536.3564	56242	1584.4336	56853	1512.5590	55939	1572.2784	56698		
1498.5080	55761	1537.2988	56254	1591.5902	56944	1515.5460	55977	1572.2779	56698		
1499.9237	55779	1539.8154	56286	1592.3795	56954	1515.6238	55978	1572.3569	56699		
1500.3148	55784	1546.2699	56368	1593.3995	56967	1515.7048	55979	1572.3568	56699		
1501.5761	55800	1549.3378	56407	1595.2901	56991	1516.4114	55988	1572.4336	56700		
1502.4431	55811	1549.4178	56408	1605.2797	57118	1516.4909	55989	1572.5145	56701		
1502.5203	55812	1551.3022	56432	1605.3595	57119	1517.4364	56001	1573.3016	56711		
1504.5661	55838	1552.3268	56445	1606.3039	57131	1519.8706	56032	1573.3771	56712		
1505.9004	55855	1554.2949	56470	1607.2497	57143	1524.8303	56095	1573.4592	56713		
1507.5560	55876	1562.3208	56572	1607.3288	57144	1528.3726	56140	1574.3229	56724		
1509.6023	55902	1562.3221	56572	1608.2734	57156	1528.4519	56141	1575.3465	56737		
1509.6795	55903	1562.3978	56573	1610.3186	57182	1528.5296	56142	1575.3465	56737		
1509.7570	55904	1562.4779	56574	1611.2627	57194	1528.6095	56143	1575.4250	56738		
1511.4895	55926	1563.5002	56587	1612.2810	57207	1528.6857	56144	1575.5020	56739		
1511.5713	55927	1564.5231	56600	1617.3184	57271	1528.7664	56145	1576.2886	56749		
1512.3591	55937	1566.3330	56623	1620.9394	57317	1530.4165	56166	1577.0770	56759		
1512.4337	55938	1568.5370	56651	1632.2740	57461	1530.4950	56167	1577.2348	56761		
1512.5917	55940	1569.3225	56661	1635.2620	57499	1530.5765	56168	1577.3137	56762		
1514.7970	55968	1569.4807	56663	1637.2295	57524	1531.3606	56178	1577.3166	56762		
1515.5830	55978	1570.3457	56674	1638.2490	57537	1531.4411	56179	1582.4268	56827		
1515.6585	55979	1570.5031	56676	1647.2206	57651	1532.3842	56191	1583.2940	56838		
1515.7390	55980	1571.2901	56686	1650.2122	57689	1532.4642	56192	1583.3729	56839		
1516.4483	55989	1571.2899	56686	1659.4158	57806	1532.5429	56193	1584.3165	56851		
1517.3906	56001	1571.3679	56687	1660.4388	57819	1533.3318	56203	1584.3953	56852		
1517.4713	56002	1571.3694	56687	1662.4069	57844	1533.4075	56204	1591.5550	56943		
1518.4955	56015	1572.2361	56698			1533.4864	56205	1593.3676	56966		
1519.9111	56033	1572.3133	56699			1534.4335	56217	1595.3274	56991		
1524.8671	56096	1572.3928	56700			1534.5092	56218	1605.2476	57117		
1528.3279	56140	1572.4706	56701			1535.6093	56232	1605.3247	57118		
1528.4067	56141	1573.3361	56712			1536.3184	56241	1605.3263	57118		

In the case of binarity there is more room for deviations from strict periodicity. We get from the light time effect (following Irwin (1959) and assuming a circular orbit), that a binary configuration realistically models the possible cyclic part of the O–C variations. The separation between the two components would be small, of the order of 1 AU. We have no good interpretation of the amplitude variations in case of binarity: as f_1 is probably a radial mode, a changing aspect angle would not give rise to amplitude variations. One could speculate that in such

a relatively close system the amplitude variations could be caused by tidal deformation of V 1162 Ori, but in this case one would expect all the detected frequencies to behave in a similar way, which is not the case. We note that such a binary system is not expected to give rise to detectable low–frequency variability in the light curves, even for a mass ratio of 1.

In conclusion, we have shown that V 1162 Ori, previously considered monoperiodic, is a multiperiodic δ Scuti star. Apart from the main mode f_1 (with harmonics), we find 5 additional frequencies in the amplitude spectrum. All these have very low amplitude and are most likely non–radial. V 1162 Ori displays period and (cyclic) amplitude variability. The main pulsational period shows a linear period change with a change rate of $(1/P)(\mathrm{d}p/\mathrm{d}t) \sim -2.4 \times 10^{-5}$ yr^{-1}. In addition, the O–C diagram reveals the presence of additional changes on the same time scale as the amplitude modulation.

The goals of the present campaign have partly been reached: we have obtained a much better knowledge of the changes present in the light curves of V 1162 Ori – but we have not been able to determine their cause. Further photometric observations are clearly needed, and so is an extensive spectroscopic investigation spanning several years to establish or reject a possible binary nature of this star.

Acknowledgements. TA and CS acknowledge financial support from the Belgian Fund for Scientific Research (FWO). This project was supported by the Flemish Ministry for Foreign Policy, European Affairs, Science and Technology, under contract BIL 98/11/52, and the National Research Foundation of South Africa. LMF acknowledges support from IUAP P4/05 financed by Belgian DWTC/SSTC. AB acknowledges support through a grant of the Conselho Nacional de Desenvolvimento Científico e Tecnológico (grant No. 301029). PVC is grateful to the Royal Observatory of Belgium for putting at his disposal material acquired by project G.0265.97 of the Fund for Scientific Research (FWO) – Flanders (Belgium); sincere thanks go to Dr. J. Cuypers. Our research has made use of the SIMBAD database operated at CDS, Strasbourg, France, and the NASA Astrophysics Data System.

References

Arentoft, T., & Sterken, C. 2000, A&A, 354, 589, Paper I
Arentoft, T., Sterken, C., & Handler, G. 2001, MNRAS, in press
Breger, M., Stich, J., Garrido, R., et al. 1993, A&A, 271, 482
Breger, M., & Pamyatnykh, A. A. 1998, A&A, 332, 958
Breger, M., Handler, G., Garrido, R., et al. 1999, A&A, 349, 225
Breger, M. 2000a, in Delta Scuti and Related Stars, ed. M. Breger, & M. Montgomery, ASP Conf. Ser., 210, 3
Breger, M. 2000b, MNRAS, 313, 129
Frandsen, S., Balona, L. A., Viskum, M., et al. 1996, A&A, 308, 132
Frandsen, S., Pigulski, A., Nuspl, J., et al. 2001, A&A, submitted
Garrido, R., Garcia–Lobo, E., & Rodriguez, E. 1990, A&A, 234, 262
Garrido, R., & Rodriguez, E. 1996, MNRAS, 281, 696
Garrido, R. 2000, in Delta Scuti and Related Stars, ed. M. Breger, & M. Montgomery, ASP Conf. Ser., 210, 67
Handler, G., Arentoft, T., Shobbrook, R. R., et al. 2000, MNRAS, 318, 511
Hintz, E. G., Joner, M. D., & Kim, C. 1998, PASP, 110, 689
Irwin, J. B. 1959, AJ, 64, 149
Lampens, P. 1985, IBVS, 2794
Lampens, P., & Van Cauteren, P. 2000, IBVS, 4857
Loumos, G. L., & Deeming, T. J. 1978, Ap&SS, 56, 2, 285
McNamara, D. H. 2000, in Delta Scuti and Related Stars, ed. M. Breger, & M. Montgomery, ASP Conf. Ser., 210, 373
Montgomery, M. H., & O'Donoghue, D. 1999, Delta Scuti Star Newsletter 13 (University of Vienna), 28
Moon, T. T., & Dworetsky, M. M. 1985, MNRAS, 217, 305
Petersen, J. O., & Christensen–Dalsgaard, J. 1996, A&A, 312, 463
Poretti, E., Antonello, E., & Le Borgne, J. F. 1990, A&A, 228, 350
Poretti, E. 2000, in Delta Scuti and Related Stars, ed. M. Breger, & M. Montgomery, ASP Conf. Ser., 210, 45
Rodriguez, E. 1999, PASP, 111, 709
Solano, E., & Fernley, J. 1997, A&AS, 122, 131
Sperl, M. 1998, Master's thesis, University of Vienna
Sterken, C. 2000, in Variable stars as essential astrophysical tools, ed. C. Ibanoglu (Kluwer Academic Publishes), 529
Sterken, C., Young, & A., Furenlid, I. 1987, A&A, 177, 150
Szeidl, B. 2000, in Delta Scuti and Related Stars, ed. M. Breger, & M. Montgomery, ASP Conf. Ser., 210, 442